

Geophysical Research Letters

RESEARCH LETTER

10.1029/2019GL084532

Key Points:

- A new experimental method is described for performing cocurrent spontaneous imbibition under elevated pressure conditions
- Spontaneous imbibition front roughening and local flow rate are described by $t^{-1/4}$ saturation-dependent scaling
- Numerically calculated capillary pressure is found to be nonzero at the residual gas saturation

Supporting Information:

- Figure S1
- Figure S2
- Figure S3
- Figure S4
- Figure S5

Correspondence to:

C. Zahasky,
chris.zahasky@gmail.com

Citation:

Zahasky, C., & Benson, S. M. (2019). Spatial and temporal quantification of spontaneous imbibition. *Geophysical Research Letters*, 46, 11,972–11,982. <https://doi.org/10.1029/2019GL084532>

Received 13 JUL 2019

Accepted 24 SEP 2019

Accepted article online 15 OCT 2019

Published online 3 NOV 2019

Corrected 27 APR 2020

This article was corrected on 27 APR 2020. See the end of the full text for details.

Spatial and Temporal Quantification of Spontaneous Imbibition

Christopher Zahasky¹  and Sally M. Benson²

¹Department of Earth Science and Engineering, Imperial College London, London, England, Now at Department of Geoscience, University of Wisconsin-Madison, Madison, WI, USA, ²Department of Energy Resources Engineering, Stanford University, Stanford, CA, USA

Abstract Spontaneous imbibition—the process of a wetting fluid displacing a nonwetting fluid purely by capillary forces—is a ubiquitous phenomenon in porous and fibrous materials. Here we present a new experimental method for quantification of spontaneous imbibition in geologic materials. This method makes it possible to perform spontaneous imbibition under elevated pressure conditions relevant to environmental and energy resource applications. Computed tomography imaging reveals a new time-independent scaling relationship that describes local imbibition rates as a function of water saturation. Imbibition capillary pressure curves are calculated with this wetting-phase pressure and flow rate characterization, with no assumptions about the functional form, end point behavior, or scaling factors. Calculated end point capillary pressure is nonzero, in agreement with recent pore-scale measurements of capillary pressure of trapped nonwetting phase. This work provides a new approach and insights into trapping and remobilization of nonwetting fluids in CO₂ storage reservoirs and contaminated groundwater aquifers.

Plain Language Summary Spontaneous flow of fluids in porous and fibrous materials is a common process that causes fluids to soak clothing, diapers, and paper and is an important process controlling the long-term movement of slow-moving fluids below the surface of the Earth. In this study, we describe a new experimental method for understanding this spontaneous fluid flow in porous rocks and map the fluid movement with a medical imaging system. We present new experimental observations of this type of flow behavior and explain the results with a mathematical model. The results of this work have important implications for how fluids interact and become trapped in carbon sequestration reservoirs, fractured geothermal reservoirs, and contaminated aquifers.

1. Introduction

Spontaneous imbibition is a ubiquitous process in everyday life, controlling physical processes from seed germination to fluids soaking paper (Miranda et al., 2010), and has important implications for two-phase flow in a range of geologic settings such as water migration in the unsaturated zone (Kao & Hunt, 1996; Zimmerman & Bodvarsson, 1989), water flooding in fractured oil reservoirs (Abd et al., 2019; Li & Firoozabadi, 2000; Ma et al., 1997; Raeesi et al., 2014; Zhou et al., 2000), and residual trapping in carbon storage reservoirs (Alyafei & Blunt, 2016; El-Maghraby & Blunt, 2013; Krevor et al., 2012; Tokunaga et al., 2013). Spontaneous imbibition is driven by capillary forces and therefore is purely dependent on the wetting behavior of fluid pairs and the unique pore-scale architecture of a porous media. As a result, accurate quantification of spontaneous imbibition has the potential to provide tremendous insights into potential changes in wettability of complex systems and the impacts of multiscale heterogeneity on two-phase flow in capillary dominated displacements.

To mathematically describe spontaneous imbibition in complex porous media, simplified models are often employed. In the classic model, a porous media is approximated as a bundle of capillary tubes and spontaneous imbibition proceeds at a rate proportional to the square root of time (Lucas, 1918; Washburn, 1921). Despite the simplicity of this approximation, experimental observations of bulk spontaneous imbibition rates in geologic porous media find similar behavior (Abd et al., 2019; Alyafei & Blunt, 2018; Fernø et al., 2013; Mason et al., 2010). While bulk imbibition rates may be described with simple approximations, dynamic imbibition behavior in simplified porous media such as Hele-Shaw cells (Hernández-Machado

et al., 2001; Soriano et al., 2005), paper (Alava et al., 2004; Zik et al., 1997), silica aerogels (Leoni et al., 2011), and glass beads (Gruener et al., 2012) have observed complex imbibition front broadening or “roughening” behavior as opposed to perfect piston-like displacement. Imbibition front roughening occurs when the fluid saturation gradient in the front decreases and becomes wider as a function of time. This front roughening during imbibition is poorly understood as it is influenced by complex interactions between local permeability/fluid mobility heterogeneity (Zik et al., 1997), dynamic effects, capillary heterogeneity, and local pore volume variation (Alava et al., 2004; Dube et al., 2007).

Unfortunately, experimental studies of dynamic in situ spontaneous imbibition displacement in geologic porous media have been limited. Experiments are challenging because external forces from experimental fluid delivery and production, to and from a porous media sample, must be avoided to maintain true spontaneous imbibition conditions. Due to experimental challenges, measurements of spontaneous imbibition in geologic materials have been limited bulk sample fluid recovery (Bartels et al., 2019; Handy, 1960; Haugen et al., 2014; Ma et al., 1997; Schmid & Geiger, 2012; Tang & Firoozabadi, 2001), nonwetting phase trapping (Chatzis & Morrow, 1984; El-Maghraby & Blunt, 2013; Reynolds et al., 2018), and imbibition front velocity (Fernø et al., 2013). Experimental studies to date have mostly been performed at ambient pressure conditions. Experimental limitations have also been unable to resolve outstanding questions related to relative permeability and capillary pressure hysteresis (Hilfer, 2006; Morrow, 1970; Pham et al., 2005; Reynolds et al., 2018), asymptotic capillary pressure characteristic behavior at low water saturation (Alyafei & Blunt, 2018), and potential nonequilibrium imbibition effects (Barenblatt et al., 2003; Hassanizadeh et al., 2002; Le Guen & Kovscek, 2006; Silin & Patzek, 2004). For complete reviews of experimental work and methods for spontaneous imbibition quantification in geologic materials see Lenormand and Eisenzimmer (1993) and Mason and Morrow (2013).

Another pressing need for spontaneous imbibition characterization is for the development of a physically unified description of capillary pressure across length scales. Pore-scale experimental studies using image-based capillary pressure characterization indicate that the physics of nonwetting phase residual trapping can be more accurately described with nonzero imbibition capillary pressure in strongly wetting systems (Armstrong et al., 2012, 2014, 2016; Herring et al., 2017; Garing et al., 2017; Li et al., 2018; Lin et al., 2018; Raeesi et al., 2014). While these experimental studies have been carried out during drainage and forced imbibition, curvature-based capillary pressure analysis has not yet been possible during spontaneous imbibition experiments. These experimental results suggest that imbibition capillary pressure is nonzero at residual nonwetting saturations, conflicting with capillary pressure curves that intersect $P_c = 0$ at the residual nonwetting saturation in strongly water-wet systems (Alyafei & Blunt, 2018; Ma et al., 1997; Pini & Benson, 2017).

In this study we present a new method for two-ends-open spontaneous imbibition. In this configuration, the radial face of a core, which is initially saturated with nonwetting phase, is sealed. One end of the core is placed in contact with wetting phase, while the other end of the core is in contact with gas from a pressurized pump. These boundary conditions produce a linear displacement cocurrent imbibition—where the wetting and nonwetting phases are flowing in the same direction. Imbibition under these conditions is termed two-ends-open free spontaneous imbibition (Dong et al., 1998; Foley et al., 2017; Haugen et al., 2014). Our new method enables cocurrent spontaneous imbibition to be performed at elevated pressures conditions. The method is demonstrated for both primary imbibition, when the core initially contains only nonwetting phase, and secondary imbibition, when the core sample is initially partially saturated with wetting phase. Spontaneous imbibition of water displacing nonwetting nitrogen gas is imaged with clinical X-ray computed tomography (X-ray CT). This imaging provides time-lapse measurements of water and gas saturations and a way to calculate local imbibition rates and imbibition front coarsening in geologic samples. Experimentally measured imbibition rates, imbibition water saturation profiles, permeability, and core-flooding water relative permeability are used to calculate imbibition capillary pressure-water saturation curves without any assumptions about the capillary pressure functional form, end point behavior, or scaling factors.

2. Novel Cocurrent Spontaneous Imbibition Experimental Method

Performing spontaneous imbibition experiments at elevated pressure and temperature conditions is important to study complex multiphase flow problems at conditions relevant to environmental and energy resource applications. The innovation presented here for performing spontaneous imbibition at elevated

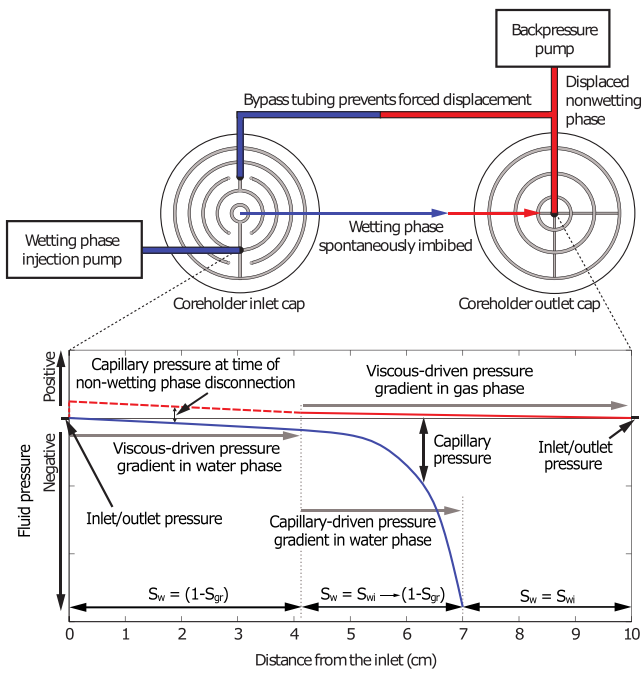


Figure 1. Illustration of inlet and outlet caps in contact with core sample and simple plumbing setup for wetting phase (blue tubing) delivery and nonwetting phase (red tubing) displacement from the core. Blue and red arrows represent wetting phase spontaneously imbibing and displacing nonwetting phase, respectively. Lower plot schematically describes differential pressure conditions in the core during spontaneous imbibition. The solid blue line is the wetting phase (water in this study). The dashed red line indicates the pressure of the disconnected nonwetting phase and the solid line describes the pressure of the connected nonwetting phase (nitrogen gas in this study). The pressure difference between the red and blue lines describes the local capillary pressure in the core.

pressure conditions relies on equalizing the pressure at the upstream and downstream ends of the core by the addition of a tube that connects the inlet and outlet of the core (top illustration in Figure 1). With shrink tubing and confining pressure sealing the cylindrical surface of the sample, this configuration prevents a differential pressure from being applied during the imbibition experiment and thus satisfies the boundary conditions of cocurrent spontaneous imbibition (Khan et al., 2018; Pooladi-Darvish & Firoozabadi, 2000). The bypass tubing is connected to the tubing between the coreholder and the backpressure pump that is maintained at a constant pressure (*Teledyne ISCO 1000D*). This enables the system to be pressurized similar to a standard core-flooding experiment where the nonwetting fluid (nitrogen gas in this study) initially present in the sample is pressurized with the backpressure pump prior to starting imbibition. When the imbibition experiment begins, the valve to the inlet of the core is opened and the wetting phase injection pump (*Teledyne ISCO 500D*) is set to a flow rate just above the spontaneous imbibition rate—determined from preimaging imbibition tests run at different flow rates. Wetting phase fluid then enters the coreholder inlet where some amount of fluid spontaneously imbibe and the excess wetting fluid is discharged into the bypass tubing. The bypass tubing was clear *Dupont Teflon PFA* 1.55-mm inner diameter tubing rated to 3,500 kPa. The water (wetting phase) pump injection rate was adjusted throughout the experiment to keep the water-air interface as static as possible in the bypass tubing, further minimizing the potential of any artificial differential pressure across the core sample. Coreholder designs are provided in the supporting information (SI).

Qualitative pressure condition during these spontaneous imbibition experiments are illustrated in the schematic in situ pressure profile in the bottom of Figure 1. In this study it is possible to orient the system horizontally due to strong viscous front stabilization forces and relatively large capillary forces in the core. In systems with larger Bond numbers (i.e., higher gravitational forces relative to capillary forces), or higher nonwetting phase fluid viscosity, it may be necessary to orient the system vertically.

With the exception of the coreholder, the experiments utilized a standard core-flooding system. A schematic and detailed description of the experimental setup used in the experiments can be found in Zahasky and Benson (2018). In all of the experiments the wetting phase was tap water and the nonwetting phase was nitrogen gas. Tap water was used to maintain moderate ionic strength conditions (salinity less than 50 mg/L) that reduce repulsive electrostatic forces (Ma et al., 2018) and therefore suppresses potential fines migration.

Prior to starting the primary imbibition experiment, the core was dried in a vacuum oven at 50 °C for a minimum of 24 hr. The confining pressure was applied with pressurized water to a value roughly 2,000 kPa higher than the pore pressure. One primary imbibition experiment was performed with a backpressure of 100 kPa, and two repeated secondary spontaneous imbibition experiments were imaged with a clinical X-ray CT *GE Lightspeed* scanner. Scans were taken every 3 to 6 min. Reconstructed and processed images had a voxel side length of 1.25 mm.

In the secondary imbibition experiments, the core had an initial water saturation of roughly 50%. The preliminary water saturation was achieved by injecting nitrogen gas at an inlet injection pressure of approximately 275 kPa for 30 min, following the completion of the previous imbibition experiment. One secondary imbibition experiment with a nitrogen backpressure of 100 kPa, the other experiment had a backpressure of 690 kPa. These duplicate experiments highlight the method repeatability and illustrate the capability of performing spontaneous imbibition experiments at elevated pressure conditions.

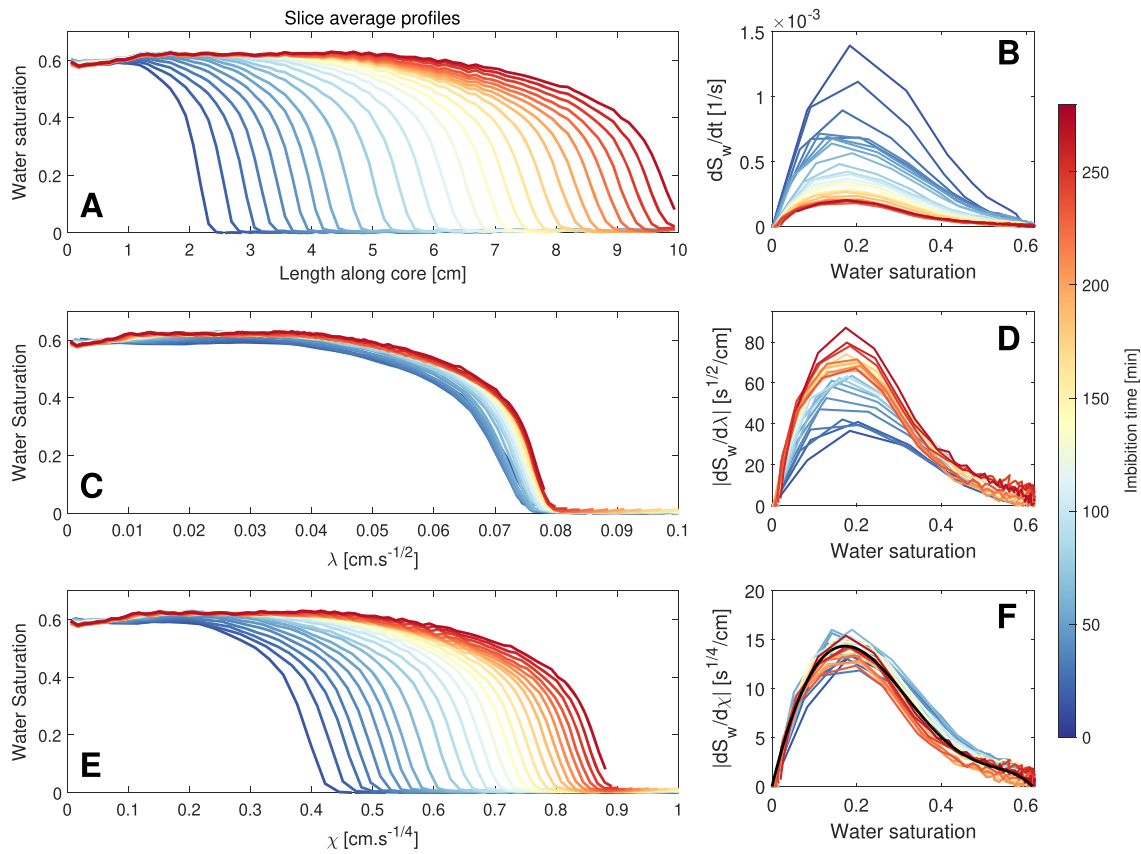


Figure 2. (a) Slice average water saturation as a function of length along core at different times during imbibition. Colored lines illustrate the time after the start of imbibition; the darkest blue line corresponds to 12.2 min, while the darkest red line indicates the scan at 264 min. (b) Derivative of water saturation with respect to time as a function of water saturation illustrated at different times during imbibition. (c) Slice average saturation scaled by the square root of time ($\lambda = x/\sqrt{t}$). (d) Absolute value of derivative of water saturation with respect to λ plotted as a function of water saturation. (e) Slice average saturation scaled by the $t^{1/4}$ ($\chi = x/t^{1/4}$). (f) Absolute value of derivative of water saturation with respect to χ plotted as a function of water saturation. The black line is the empirical fit given by equation (4). The absolute value of the derivatives in (d) and (f) are plotted for comparison with derivative in plot (b).

3. Computed Tomography Imaging of Dynamic Spontaneous Imbibition Experiments

X-ray CT was used to quantify three-dimension time-lapse water saturation during spontaneous imbibition in a 5 cm diameter, 10 cm long Berea sandstone core (additional details of sample characterization are provided in the SI). The dynamic water saturation measurements were then used to calculate total and local imbibition rates. The slice (ζ) average water saturation as a function of time ($S_w(\zeta, t)$) was calculated using the classic X-ray CT linear scaling expressions saturation (Akin & Kovscek, 2003)—detailed equations are provided in the SI. The upper plot in Figure 2a illustrates the dynamic slice-averaged water saturation measured during the primary spontaneous imbibition experiment. The slice average saturation profiles in Figure 2a illustrate a compact imbibition front geometry due to the viscous stability of water/air displacement (Alyafei et al., 2016; Dong et al., 1998; Haugen et al., 2014; Le Guen & Kovscek, 2006; Schembre & Kovscek, 2006; Wickramathilaka et al., 2011; Zhao et al., 2017).

The change in water saturation in each slice ($dS = S_w(\zeta, t_n) - S_w(\zeta, t_{n-1})$) divided by the change in time ($dt = t_n - t_{n-1}$) is proportional to the imbibition rate. The water saturation derivative as a function of local water saturation as the imbibition front migrates through the core is plotted in Figure 2b. Imbibition front broadening or “roughening” behavior is apparent in Figure 2b because the rate of water saturation change with time is decreasing across the imbibition front as water imbibes into the core. Front roughing is also apparent from Figure 2a because the slope of the water saturation front along the length of the core is decreasing with time. Imbibition front analysis was also performed on a 1-cm² subvolume running along

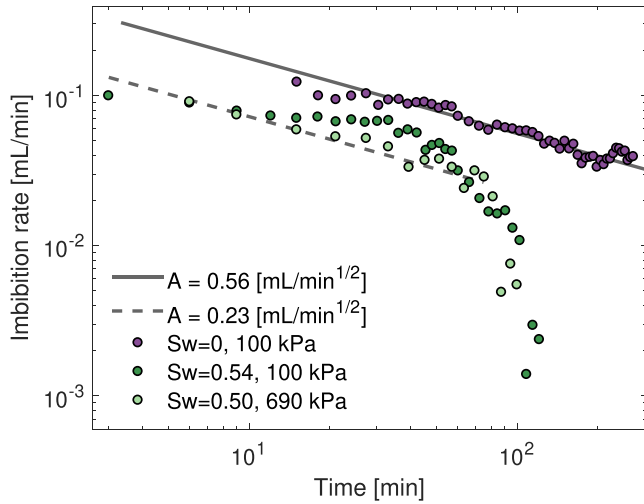


Figure 3. Water imbibition rate as a function of time for the primary imbibition experiment (purple points) and repeated secondary spontaneous imbibition experiments at 100 and 690 kPa gas phase pressure conditions (dark green and light green points, respectively). The core-averaged initial water saturation (S_{wi}) for each experiment is indicated in the legend. The total primary water imbibition rate can be described by $Q_{imb}^w(t) = At^{-1/2}$ as detailed by McWhorter and Sunada (1990). A has units of $\text{ml}/\text{min}^{1/2}$ for simplified comparison with experimental measurement units.

the length of the core to verify that the front roughening was not a result of a spatially variable imbibition. A summary of these data is included in the SI.

Typical analytical imbibition scaling analysis (Alyafei et al., 2016; McWhorter & Sunada, 1990; Schembre & Kovscek, 2006; Zimmerman & Bodvarsson, 1991) relies on scaling the length dimension parallel to the direction of flow by the square root of time ($\lambda = x/\sqrt{t}$). Plotting the saturation profiles as a function of λ allows the tip of the imbibition front to collapse to a single value as demonstrated in Figure 2c. Close examination of the square root of time scaling of the saturation profiles in Figure 2c indicate that this scaling approach does not describe the roughening of the imbibition front. This is highlighted in the derivative analysis of λ (as defined by equation (1)) and plotted in Figure 2d.

$$\frac{dS_w}{dt} = \frac{dS_w}{d\lambda} \frac{d\lambda}{dt} = -\frac{dS_w}{d\lambda} \frac{x}{2t^{3/2}} \quad (1)$$

Instead, we find that the imbibition front roughening scales by $t^{-1/4}$. Water saturation as a function of length scaled by $t^{-1/4}$, here termed χ , is shown in Figure 2e. The derivative of water saturation as a function of χ is explicitly defined in equations (2) and 3.

$$\frac{dS_w}{dt} = \frac{dS_w}{d\chi} \frac{d\chi}{dt} = -\frac{dS_w}{d\chi} \frac{x}{4t^{5/4}} \quad (2)$$

$$\frac{dS_w}{d\chi} = -\frac{dS_w}{dt} \frac{4t^{5/4}}{x} \quad (3)$$

The results of the absolute value of $dS_w/d\chi$ as a function of water saturation are plotted in Figure 2f at each time corresponding to the saturation profiles in Figure 2a. The curves in Figure 2f at different times approximately collapse to one curve that can be fit by the empirical function given by equation (4) (black line in Figure 2f).

$$\left| \frac{dS_w}{d\chi} \right| = -2267S_w^5 + 2611S_w^4 - 281.3S_w^3 - 581.5S_w^2 + 181.0S_w \quad (4)$$

This fifth-order polynomial was found to be the simplest empirical function to describe the complex time-independent relationship between local imbibition rate and in situ water saturation.

The solid gray line in Figure 3 highlights that while the front coarsening scales by $t^{-1/4}$, the total water primary imbibition rate into the core closely follows the inverse square root relationship that has been measured in previous studies (Alyafei & Blunt, 2018; Ma et al., 1997; Mattax & Kyte, 1962). While the secondary imbibition data is complicated by spatial variability of initial water saturation, the imbibition flux roughly follows an inverse square root relationship at early time (dashed gray line Figure 3). As the imbibing front approaches the outlet face boundary the imbibition flux decreases exponentially as observed by Li and Firoozabadi (2000). Figure 3 illustrates the near-identical imbibition flow rate behavior of the secondary spontaneous imbibition experiments performed at different pore pressure conditions, highlighting experimental repeatability and capability at elevated pressures.

4. Calculation of Imbibition Capillary Pressure

Improved understanding of the impact of imbibition rate, front roughening, end point capillary pressure behavior, and the implementation of capillary pressure imbibition experimental observations into numerical simulators requires quantification of capillary pressure as a function of water saturation. In this section we describe a new quasistatic, one-dimensional approach to numerically calculate the in situ water-phase pressure during spontaneous imbibition into dry samples.

This new approach calculates the wetting-phase pressure across the length of the core at a single instant in time using the experimentally constrained flow rate and fluid mobility conditions. Specifically, the algorithm utilizes experimentally measured imbibition rates, imbibition water saturation profiles, permeability, and water relative permeability estimates. This quasistatic approach, where the pressure is calculated at one instant in time, is a valid assumption because the maximum measured imbibition rate is less than 0.25 ml/min and the first pressure profile is not calculated until the imbibition rate falls below 0.1 ml/min.

To enable a simplified calculation of wetting phase pressure, the influence of nitrogen displacement and the nonwetting phase gas pressure conditions are neglected. The viscous resistance of nitrogen is negligible because of the very low imbibition rates and because the viscosity of nitrogen gas is several orders of magnitude lower than water. This condition has been justified by previous analysis of experimental and numerical spontaneous imbibition data that indicates that gas relative permeability has little influence on displacement rates (Alyafei et al., 2016) and that the pressure drop in the gas phase is negligible (Beckner et al., 1987; Handy, 1960; McWhorter & Sunada, 1990; Pooladi-Darvish & Firoozabadi, 2000). By assuming that the nonwetting pressure is approximately constant throughout the core, the imbibition capillary pressure can be determined as a function of water saturation.

During spontaneous imbibition, capillary pressure drives wetting phase displacement of the nonwetting phase, while the fluid viscosity, intrinsic permeability, and relative permeability determine the resistance to this displacement process. As a result of this complex nonlinear interaction, unique parameterization of relative permeability during spontaneous imbibition is challenging (Alyafei et al., 2016; Lombard et al., 2002). Previous forced imbibition and drainage experiments in Berea sandstone samples indicate that while nonwetting relative permeability exhibits strong hysteresis, water relative permeability in gas-water systems follows a nonhysteretic curve (e.g., Figures 9 and 11 in Ruprecht et al., 2014) or exhibits subtle hysteresis (e.g., Figure 18 in Akbarabadi & Piri, 2013). In this study, we therefore utilize relative permeability measurements taken during separate drainage experiments to approximate a unique capillary pressure solution.

Implemented in Matlab, the local capillary pressure during spontaneous imbibition is calculated using the following workflow:

1. *Measure water saturation profile along core:* An analytical function is fit to the one-dimensional water saturation profile ($S_w(x, t_n)$) during spontaneous imbibition at a specific time (t_n), as measured with the clinical X-ray CT scanner.
2. *Calculate effective permeability of wetting phase:* The effective permeability ($k_e(S_w)$) is determined by multiplying the core-averaged permeability (k_{core}) and the water relative permeability ($k_e(S_w) = k_{core}k_{rw}(S_w)$). The water relative permeability is determined from the experimentally measured drainage relative permeability data.
3. *Assign initial conditions in imbibition front:* Grid cell (i) water accumulation rates ($dV_{w,i}/dt$) are determined at time t_n using the scaling relation to water saturation (dS_w/dx)—described in section 3.

$$\frac{dV_{w,i}}{dt} = \begin{cases} \varphi_i \frac{dS_w}{dx} \frac{x}{4t_n^{5/4}}, & 0 \leq S_w < 1 - S_{gr} \\ 0, & S_w = 1 - S_{gr} \end{cases} \quad (5)$$

Here φ_i is the pore volume of grid cell i and x is the distance of the grid cell from the inlet in centimeters. S_{gr} is the residual gas saturation.

4. *Assign boundary conditions to core inlet:* To strictly enforce mass balance, the inlet face (left side of the model) imbibition flow rate ($Q_{imb}^w(t)$) is set equal the sum of the accumulation rates in calculated in the grid cells in the imbibition front (as determined in the previous step).

$$Q_{imb}^w(x = 0, t_n) = \sum_i \frac{dV_{w,i}}{dt} \quad (6)$$

Alternatively, if the front roughening is more variable during imbibition, the grid cell water accumulation rates ($dV_{w,i}/dt$) may be rescaled to perfectly match the total imbibition rate measured experimentally (i.e., the values in Figure 3).

5. *Solve system of finite-difference equations to determine wetting phase pressure:* The foundational equation for the finite difference model is the water mass balance across each face of a given grid cell. The water fluxes across these interfaces are approximated using Darcy's Law, here assuming constant water density

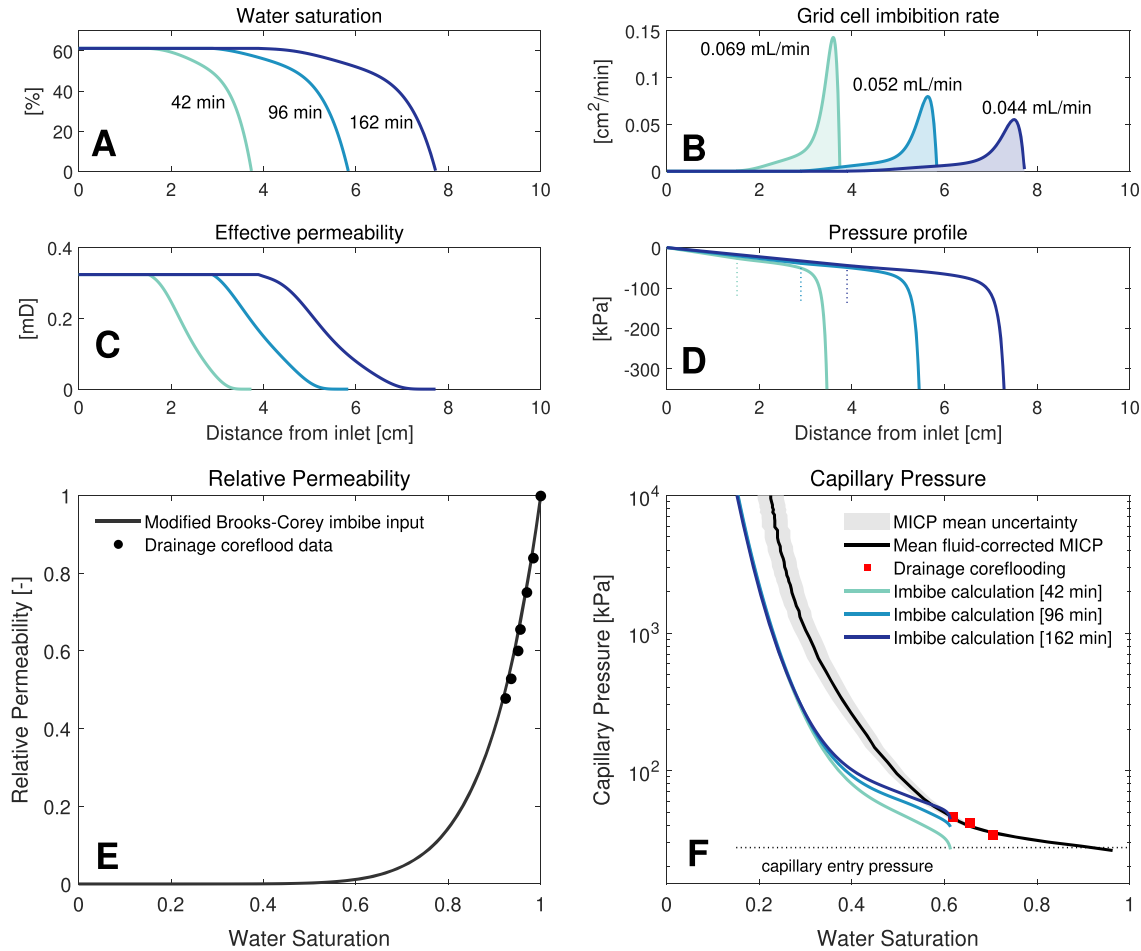


Figure 4. (a) Slice average water saturation profiles across the core at imbibition times of 42, 96, and 162 min. (b) Accumulation rate in the grid cells in the imbibition front calculated using the water saturation profiles (Figure 4a) and equation (5). The total calculated imbibition rate is specified by text above each line. Imbibition rate is plotted as cm^2/min so that the integral (shaded region) of the rate illustrates the total water imbibition rate ($Q_{\text{imb}}^{\text{tot}}(t)$). (c) Effective permeability as a function of distance along the core using the water saturation profiles in Figure 4a and the relative permeability function described in Figure 4e. (d) Simulated pressure profile in the water phase. Dashed vertical lines indicate transition from viscous pressure gradient to capillary-driven pressure gradient (see illustration in Figure 1). The pressure at these lines indicates the end point capillary when the nonwetting phase becomes disconnected. (e) Laboratory drainage relative permeability measurements (black points) and the water relative permeability curve fit used to model water pressure profile across the core. The experimental marker size is proportional to relative permeability measurement error—specifically two standard deviations of measurement noise. (f) Colored lines show calculated imbibition capillary pressure as a function of saturation. The black line is the mean of five fluid-corrected mercury injection capillary pressure (MICP) curves and the red points show core-flooding drainage capillary pressure measurements. The shaded MICP uncertainty illustrates the error arising from bulk volume dimension measurements and helium pycnometer measurement variation (see supporting information for details). The saturation measurement error decreases at increasing water saturation.

and viscosity. The transmissibility between adjacent grid cells and $(p_{i-1} - p_i)$ is the pressure difference between grid cell centers of adjacent cells. The explicit grid cell transmissibility terms—calculated as the harmonic mean across the interface between grid cells—are contained in the **A** matrix. The explicit source (inlet boundary conditions) and accumulation terms (imbibition front initial conditions) are described by the **b** vector.

$$\mathbf{A}^n \mathbf{p}^{n+1} = \mathbf{b}^n \quad (7)$$

The system is solved for **p** in Matlab with the backslash operator.

6. *Calculate capillary pressure:* The capillary pressure ($P_{c,i}(S_w)$) for each grid cell (i) is calculated by taking the difference between the inlet water pressure and the local grid cell pressure values (p_i).

$$P_{c,i}(S_w) = \{ P_{\text{inlet}} - p_i(S_w), 0 \leq S_w < 1 - S_{\text{gr}} \quad (8)$$

In grid cells with $S_w = 1 - S_{\text{gr}}$ the nonwetting phase is disconnected and the calculated pressure difference no longer reflects the capillary pressure.

It is important to reemphasize that the inlet water phase pressure is equal to the gas pressure at the outlet ($p_{\text{inlet}} = p_{\text{outlet}}$) of the coreholder due to the tubing connection—neglecting the minimal capillary pressure in the bypass tubing. Under these conditions, the grid cell pressure in the imbibition front reflects the capillary pressure required to induce the experimentally measured spontaneous imbibition flow rate conditions (see schematic in Figure 1 for illustration).

The impact of gravity on pressure distribution is neglected because the experiments were performed horizontally. In a vertically oriented core, gravity would have to be accounted for in the capillary pressure calculation (Bartels et al., 2019; Khan et al., 2018). The detailed governing equations, model formulation, and numerical implementation for this model can be found in the SI.

4.1. Imbibition Capillary Pressure Model Results From Experimental Data

An analytical function is used to describe the water saturation to enable finer discretization ($1 \times 1 \times 2,000$ grid cells) of the model along the axis of the core than is possible from the experimentally imaged voxel data (88 slices \times 1.25 mm in width). The dynamic portion of the experimental slice-averaged water saturation profiles are fit with a fifth-order polynomial. Figure 4a shows three saturation profiles at imbibition times of 42, 96, and 162 min. Grid cell accumulation terms ($dV_{w,i}/dt$) are assigned to cells located in the imbibition front, as determined by grid cells with saturation values not equal to $1-S_{\text{gr}}$. Calculated imbibition rates in the front are plotted in Figure 4b. The calculated accumulation rate sums, specified in the text annotation in Figure 4b, are approximately equal to the experimentally measured core-averaged imbibition rates.

The effective permeability of the model along the axis of the core (Figure 4c) was calculated using the core-averaged permeability ($k_{\text{core}} = 23$ mD) multiplied by the drainage relative permeability. The water relative permeability function is described by $k_{\text{rw}} = (S_w)^{8.7}$, as shown in Figure 4e. The raw relative permeability data and measurement methodology are provided in the SI. The relative permeability function does not include an irreducible gas saturation because the model is describing primary imbibition, and therefore, the initial gas saturation is equal to 0.

Figures 4d and 4f illustrate the calculated pressure profile along the core and the calculated imbibition capillary pressure versus water saturation, respectively. The shapes of the calculated pressure profile agree well with previous simulation studies of imbibing phase pressure distributions (Li et al., 2006; Pooladi-Darvish & Firoozabadi, 2000). The relative permeability and calculated capillary pressure curves are also consistent with analytical solutions. A comparison of the numerically calculated capillary pressure and analytical solution described in Alyafei et al. (2016) is available in the SI.

5. Discussion and Conclusion

This study describes a new experimental method for performing spontaneous imbibition experiments in geologic porous media at elevated pressure conditions relevant to pressing environmental and engineering challenges. Dynamic primary and secondary spontaneous imbibition experiments were performed and local water saturation was measured with clinical X-ray CT. The experiments highlight primary and secondary spontaneous imbibition repeatability and method capability at elevated pore pressures.

Analysis of the primary spontaneous imbibition experiment reveals the first quantitative measurements of imbibition front roughening, or broadening of the imbibition front, in geologic porous media. These experiments indicate a roughening behavior that scales with $t^{1/4}$. The empirical scaling relationship used to describe the time-independent behavior of the local imbibition rate as a function of in situ water saturation is a complex interaction of pore-scale fluctuations in capillary forces, permeability and relative permeability heterogeneity, potential dynamic behavior, fluid characteristics, and viscous force dampening (Soriano et al., 2005). Future work is necessary to determine how the form of this imbibition rate-saturation function changes as a result of the magnitude of local capillary forces, wettability, imbibition rate, fluid viscosity, and different capillary and permeability heterogeneity.

Experimental measurements of dynamic fluid saturation enable parameterization of a quasistatic numerical model to calculate local water pressure conditions during spontaneous imbibition. With this model, pressure profiles and corresponding capillary pressure are calculated directly from the experimental data. Results of the model indicate that the capillary pressure at the residual gas saturation is greater than zero. The entry pressure determined from mercury injection capillary pressure and drainage core-flooding data was $P_0 = 27.6$ kPa, while the end point capillary pressure during imbibition was $P_0(t = 42\text{min}) = 26.7$

kPa, $P_0(t = 96\text{min}) = 39.0$ kPa, and $P_0(t = 162\text{min}) = 44.3$ kPa, as indicated in Figure 4f. This increasing end point pressure as the imbibition front approaches the end of the core is likely a combination of capillary heterogeneity and parameterization measurement error. Previous permeability inversion studies using this same core have indicated that the region near the outlet has a slightly lower permeability (Vasco et al., 2018), and therefore likely slightly higher capillary pressure. It is also important to note that capillary pressure end point is sensitive to water relative permeability, total imbibition rate, and water saturation measurement error.

The numerical method described in this study is an improvement over existing water-air spontaneous imbibition modeling techniques because it is easy to implement and because the capillary pressure is discretely calculated. The formulation enables very steep capillary pressure gradients to be calculated as highlighted in Figure 4f. These gradients are challenging to model with standard reservoir simulation approaches due to the prohibitively fine grids required (Pooladi-Darvish & Firoozabadi, 2000; Ruth et al., 2015; Settari & Aziz, 1975). The benefit of this numerical method over analytical methods is that it does not require simplifying and restrictive assumptions about the shape of the saturation profile (Haugen et al., 2014), characteristic curve functional form (Fokas & Yortsos, 1982; Kashchiev & Firoozabadi, 2003; Zimmerman & Bodvarsson, 1989, 1991), imbibition rate scaling (Alyafei & Blunt, 2018; Alyafei et al., 2016; Foley et al., 2017; McWhorter & Sunada, 1990), or relative degrees of cocurrent and countercurrent flow (McWhorter & Sunada, 1990; Schmid et al., 2011).

The end point capillary pressure calculations provide a new way to bridge continuum-scale capillary pressure measurements with pore-scale simulation and experimental measurements of nonzero capillary pressures. The experimental method presented here combined with in situ imaging will enable future studies of spontaneous imbibition experiments at a range of spatial scales, wettability conditions, and with higher-pressure fluids and gases such as supercritical CO_2 . These types of studies will help elucidate fundamental questions about the relationship between connected and disconnected nonwetting phase pressure, and how nonwetting phase ganglia capillary pressure is related to capillary entry pressure during secondary imbibition. These studies will aid in improving understanding of an array of capillary-dominated fluid transport and displacement processes in the subsurface such as CO_2 capillary trapping in carbon storage reservoirs and nonaqueous phase liquid immobilization and remediation.

Acknowledgments

Experimental data and Matlab codes for generating Figures 2 and 3 are available on the Stanford Digital Repository (<https://purl.stanford.edu/rq760rw7552>). This work was funded by the Global Climate Energy Project, the Stanford Center for Carbon Storage, and the Stanford University Department of Energy Resources Engineering. This work was supported as part of the Center for Mechanistic Control of Water-Hydrocarbon-Rock Interactions in Unconventional and Tight Oil Formations (CMC-UF), an Energy Frontier Research Center funded by the U.S. Department of Energy, Office of Science under DOE (BES) Award DE-SC0019165.

References

- Abd, A. S., Elhafyan, E., Rafey, A., Alnoush, W., Blunt, M. J., & Alyafei, N. (2019). Journal of petroleum science and engineering: A review of the phenomenon of counter-current spontaneous imbibition : Analysis and data interpretation. *Journal of Petroleum Science and Engineering*, *180*, 456–470. <https://doi.org/10.1016/j.petrol.2019.05.066>
- Akbarabadi, M., & Piri, M. (2013). Advances in water resources relative permeability hysteresis and capillary trapping characteristics of supercritical CO_2 /brine systems : An experimental study at reservoir conditions. *Advances in Water Resources*, *52*, 190–206. <https://doi.org/10.1016/j.advwatres.2012.06.014>
- Akin, S., & Kovscek, A. R. (2003). Computed tomography in petroleum engineering research. *Applications of X-ray Computed Tomography in the Geosciences*, *215*, 23–38.
- Alava, M., Dubé, M., & Rost, M. (2004). Imbibition in disordered media. *Advances in Physics*, *53*(2), 83–175. <https://doi.org/10.1080/00018730410001687363>
- Alyafei, N., Al-Menhali, A., & Blunt, M. J. (2016). Experimental and analytical investigation of spontaneous imbibition in water-wet carbonates. *Transport in Porous Media*, *115*, 189–207. <https://doi.org/10.1007/s11242-016-0761-4>
- Alyafei, N., & Blunt, M. J. (2016). The effect of wettability on capillary trapping in carbonates. *Advances in Water Resources*, *90*, 36–50. <https://doi.org/10.1016/j.advwatres.2016.02.001>
- Alyafei, N., & Blunt, M. J. (2018). Estimation of relative permeability and capillary pressure from mass imbibition experiments. *Advances in Water Resources*, *115*, 88–94. <https://doi.org/10.1016/j.advwatres.2018.03.003>
- Armstrong, R. T., Georgiadis, A., Ott, H., Klemin, D., & Berg, S. (2014). Critical capillary number: Desaturation studied with fast X-ray computed microtomography. *Geophysical Research Letters*, *41*, 55–60. <https://doi.org/10.1002/2013GL058075>
- Armstrong, R. T., McClure, J. E., Berrill, M. A., Rücker, M., Schlüter, S., & Berg, S. (2016). Beyond Darcy's law: The role of phase topology and ganglion dynamics for two-fluid flow. *Physical Review E - Statistical, Nonlinear, and Soft Matter Physics*, *94*(4), 1–10. <https://doi.org/10.1103/PhysRevE.94.043113>
- Armstrong, R. T., Porter, M. L., & Wildenschild, D. (2012). Linking pore-scale interfacial curvature to column-scale capillary pressure. *Advances in Water Resources*, *46*, 55–62. <https://doi.org/10.1016/j.advwatres.2012.05.009>
- Barenblatt, G. I., Patzek, T. W., & Silin, D. B. (2003). The mathematical model of nonequilibrium effects in water-oil displacement. *SPE Journal*, *8*(04), 409–416. <https://doi.org/10.2118/87329-PA>
- Bartels, W., Rücker, M., Boone, M., Bultreys, T., Mahani, H., Berg, S., et al. (2019). Imaging spontaneous imbibition in full Darcy-scale samples at pore-scale resolution by fast X-ray tomography. *Water Resources Research*, *55*, 7072–7085. <https://doi.org/10.1029/2018WR024541>
- Beckner, B. L., Ishimoto, K., Yamaguchi, S., Firoozabadi, A., & Aziz, K. (1987). Imbibition-Dominated Matrix-Fracture Fluid Transfer in Dual Porosity Simulators. This paper was prepared for presentation at the 62nd Annual Technical Conference and Exhibition of the Society of Petroleum Engineers held in Dallas, TX, September 27–30, 1987. (SPE 16981).

- Chatzis, I., & Morrow, N. R. (1984). Correlation of capillary number relationships for sandstone. *Society of Petroleum Engineers Journal*, 24(05), 555–562. <https://doi.org/10.2118/10114-PA>
- Dong, M., Dullien, F. a. L., & Zhou, J. (1998). Characterization of waterflood saturation profile histories by the 'Complete' Capillary Number. *Transport in Porous Media*, 31(2), 213–237. <https://doi.org/10.1023/A:1006565621860>
- Dube, M., Daneault, C., Vuorinen, V., Alava, M., & Rost, M. (2007). Front roughening in three-dimensional imbibition. *The European Physical Journal B*, 26, 15–26. <https://doi.org/10.1140/epjb/e2007-00085-7>
- El-Maghraby, R. M., & Blunt, M. J. (2013). Residual CO₂ trapping in Indiana limestone. *Environmental Science and Technology*, 47(1), 227–233. <https://doi.org/10.1021/es304166u>
- Fernø, M. A., Haugen, Å., Wickramathilaka, S., Howard, J., Graue, A., Mason, G., & Morrow, N. R. (2013). Magnetic resonance imaging of the development of fronts during spontaneous imbibition. *Journal of Petroleum Science and Engineering*, 101, 1–11. <https://doi.org/10.1016/j.petrol.2012.11.012>
- Fokas, A. S., & Yortsos, Y. C. (1982). On the exactly solvable equation occurring in two-phase flow in porous media. *SIAM Journal of applied math*, 42(2), 318–332.
- Foley, A. Y., Nooruddin, H. A., & Blunt, M. J. (2017). The impact of capillary backpressure on spontaneous counter-current imbibition in porous media. *Advances in Water Resources*, 107, 405–420. <https://doi.org/10.1016/j.advwatres.2017.04.012>
- Garing, C., de Chalendar, J. A., Voltolini, M., Ajo-Franklin, J. B., & Benson, S. M. (2017). Pore-scale capillary pressure analysis using multi-scale X ray micromotography. *Advances in Water Resources*, 104, 223–241. <https://doi.org/10.1016/j.advwatres.2017.04.006>
- Gruener, S., Sadjadi, Z., Hermes, H. E., Kityk, A. V., Knorr, K., & Egelhaaf, S. U. (2012). Anomalous front broadening during spontaneous imbibition in a matrix with elongated pores. *Proceedings of the National Academy of Sciences*, 109(26), 10,245–10,250. <https://doi.org/10.1073/pnas.1119352109>
- Handy, L. L. (1960). Determination of effective capillary pressures for porous media from imbibition data. *Petroleum Transactions, AIME*, 219, 75–80. <http://www.aimehq.org/search/docs/Volume219/219-22.pdf>
- Hassanizadeh, S. M., Celia, M. A., & Dahle, H. K. (2002). Dynamic effect in the capillary pressure-saturation relationship and its impacts on unsaturated flow. *Vadose Zone Journal*, 1(1), 38. <https://doi.org/10.2136/vzj2002.0038>
- Haugen, A., Fernø, M. A., Mason, G., & Morrow, N. R. (2014). Capillary pressure and relative permeability estimated from a single spontaneous imbibition test. *Journal of Petroleum Science and Engineering*, 115, 66–77. <https://doi.org/10.1016/j.petrol.2014.02.001>
- Hernández-Machado, A., Soriano, J., Lacasta, A. M., Rodríguez, M. A., Ramírez-Piscina, L., & Ortín, J. (2001). Interface roughening in Hele-Shaw flows with quenched disorder: Experimental and theoretical results. *EPL (Europhysics Letters)*, 55(2), 194. <http://stacks.iop.org/0295-5075/55/i=2/a=194>
- Herring, A. L., Middleton, J., Walsh, R., Kingston, A., & Sheppard, A. (2017). Flow rate impacts on capillary pressure and interface curvature of connected and disconnected fluid phases during multiphase flow in sandstone. *Advances in Water Resources*, 107, 460–469. <https://doi.org/10.1016/j.advwatres.2017.05.011>
- Hilfer, R. (2006). Macroscopic capillarity and hysteresis for flow in porous media. *Physical Review E - Statistical, Nonlinear, and Soft Matter Physics*, 73(1), 0–9. <https://doi.org/10.1103/PhysRevE.73.016307>
- Kao, C. S., & Hunt, J. R. (1996). Prediction of wetting front movement during one-dimensional infiltration into soils. *Water Resources Research*, 32(1), 55–64. <https://doi.org/10.1029/95WR02974>
- Kashchiev, D., & Firoozabadi, A. (2003). Analytical solutions for 1D countercurrent imbibition in water-wet media. *SPE Journal*, 8(04), 401–408. <https://doi.org/10.2118/87333-PA>
- Khan, A. S., Siddiqui, A. R., Abd, A. S., & Alyafei, N. (2018). Guidelines for numerically modeling co- and counter-current spontaneous imbibition. *Transport in Porous Media*, 124(3), 743–766. <https://doi.org/10.1007/s11242-018-1093-3>
- Krevor, S. C. M., Pini, R., Zuo, L., & Benson, S. M. (2012). Relative permeability and trapping of CO₂ and water in sandstone rocks at reservoir conditions. *Water Resources Research*, 48, W02532. <https://doi.org/10.1029/2011WR010859>
- Le Guen, S. S., & Kovscek, A. R. (2006). Nonequilibrium effects during spontaneous imbibition. *Transport in Porous Media*, 63(1), 127–146. <https://doi.org/10.1007/s11242-005-3327-4>
- Lenormand, R., & Eisenzimmer (1993). A novel method for the determination of semi dynamic Pc.pdf.
- Leoni, F., Kierlik, E., Rosinberg, M. L., & Tarjus, G. (2011). Spontaneous imbibition in disordered porous solids: A theoretical study of helium in silica aerogels. *Langmuir*, 27(13), 8160–8170. <https://doi.org/10.1021/la201146h>
- Li, K., & Firoozabadi, A. (2000). Experimental study of wettability alteration to preferential gas-wetting in porous media and its effects. *SPE Reservoir Evaluation & Engineering*, 3(2), 139–149. <https://doi.org/10.2118/62515-PA>
- Li, Y., Ruth, D., Mason, G., & Morrow, N. R. (2006). Pressures acting in counter-current spontaneous imbibition. *Journal of Petroleum Science and Engineering*, 52(1-4), 87–99. <https://doi.org/10.1016/j.petrol.2006.03.005>
- Li, T., Schlüter, S., Dragila, M. I., & Wildenschild, D. (2018). An improved method for estimating capillary pressure from 3D microtomography images and its application to the study of disconnected nonwetting phase. *Advances in Water Resources*, 114, 249–260. <https://doi.org/10.1016/j.advwatres.2018.02.012>
- Lin, Q., Bijeljic, B., Pini, R., Blunt, M. J., & Krevor, S. (2018). Imaging and measurement of pore-scale interfacial curvature to determine capillary pressure simultaneously with relative permeability. *Water Resources Research*, 54, 7046–7060. <https://doi.org/10.1029/2018WR023214>
- Lombard, J.-M., Egermann, P., & Lenormand, R. (2002). Measurement of capillary pressure curves at reservoir conditions. *Society of Core Analysts*, 09, 1–16.
- Lucas, R. (1918). Über das Zeitgesetz des kapillaren Aufstiegs von Flüssigkeiten. *Colloid Polymer Science*, 23(1), 15–22.
- Ma, C., Huangfu, X., He, Q., Ma, J., & Huang, R. (2018). Deposition of engineered nanoparticles (ENPs) on surfaces in aquatic systems: A review of interaction forces, experimental approaches, and influencing factors. *Environmental Science and Pollution Research*, 25(33), 33,056–33,081. <https://doi.org/10.1007/s11356-018-3225-2>
- Ma, S., Morrow, N. R., & Zhang, X. (1997). Generalized scaling of spontaneous imbibition data for strongly water-wet systems. *Journal of Petroleum Science and Engineering*, 4105(97), 165–178.
- Mason, G., Fischer, H., Morrow, N. R., Johannesen, E., Haugen, Å., Graue, A., & Fernø, M. A. (2010). Oil production by spontaneous imbibition from sandstone and chalk cylindrical cores with two ends open. *Energy and Fuels*, 24(2), 1164–1169. <https://doi.org/10.1021/ef901118n>
- Mason, G., & Morrow, N. R. (2013). Developments in spontaneous imbibition and possibilities for future work. *Journal of Petroleum Science and Engineering*, 110, 268–293. <https://doi.org/10.1016/j.petrol.2013.08.018>
- Mattax, C. C., & Kyte, J. R. (1962). Imbibition oil recovery from fractured, water-drive reservoir. *Society of Petroleum Engineers Journal*, 2(02), 177–184. <https://doi.org/10.2118/187-PA>

- McWhorter, D. B., & Sunada, D. K. (1990). Exact integral solutions for two-phase flow. *Water Resources Research*, 26(3), 399–413. <https://doi.org/10.1029/WR026i003p00399>
- Miranda, A. M., Menezes-Sobrinho, I. L., & Couto, M. S. (2010). Spontaneous imbibition experiment in newspaper sheets. *Physical Review Letters*, 104(8), 1–4. <https://doi.org/10.1103/PhysRevLett.104.086101>
- Morrow, N. R. (1970). Physics and thermodynamics of capillary action in porous media. *Industrial & Engineering Chemistry*, 62(6), 32–56. <https://doi.org/10.1021/ie50726a006>
- Pham, H. Q., Fredlund, D. G., & Barbour, S. L. (2005). A study of hysteresis models for soil-water characteristic curves. *Canadian Geotechnical Journal*, 42(6), 1548–1568. <https://doi.org/10.1139/t05-071>
- Pini, R., & Benson, S. M. (2017). Capillary pressure heterogeneity and hysteresis for the supercritical CO₂/water system in a sandstone. *Advances in Water Resources*, 108, 277–292. <https://doi.org/10.1016/j.advwatres.2017.08.011>
- Pooladi-Darvish, M., & Firoozabadi, A. (2000). Cocurrent and countercurrent imbibition in a water-wet matrix block. *Spe, March*, 3–11. <https://doi.org/10.2118/38443-PA>
- Raeesi, B., Morrow, N. R., & Mason, G. (2014). Capillary pressure hysteresis behavior of three sandstones measured with a multistep outflow/inflow apparatus. *Vadose Zone Journal*, 13(3), 1–12. <https://doi.org/10.2136/vzj2013.06.0097>
- Reynolds, C. A., Blunt, M. J., & Krevor, S. (2018). Multiphase flow characteristics of heterogeneous rocks from CO₂ storage reservoirs in the United Kingdom. *Water Resources Research*, 54, 729–745. <https://doi.org/10.1002/2017WR021651>
- Ruprecht, C., Pini, R., Falta, R., Benson, S., & Murdoch, L. (2014). Hysteretic trapping and relative permeability of CO₂ in sandstone at reservoir conditions. *International Journal of Greenhouse Gas Control*, 27, 15–27. <https://doi.org/10.1016/j.ijggc.2014.05.003>
- Ruth, D. W., Mason, G., Ferno, M. A., Haugen, A., Morrow, N. R., & Arabjamaloei, R. (2015). Numerical simulation of combined co-current/counter-current spontaneous imbibition. This paper was prepared for presentation at the International Symposium of the Society of Core Analysts held in St. John's, Newfoundland and Labrador, Canada, 16–21 August, 2015. (SCA2015-002).
- Schembre, J. M., & Kovscek, A. R. (2006). Estimation of dynamic relative permeability and capillary pressure from countercurrent imbibition experiments. *Transport in Porous Media*, 65(1), 31–51. <https://doi.org/10.1007/s11242-005-6092-5>
- Schmid, K. S., & Geiger, S. (2012). Universal scaling of spontaneous imbibition for water-wet systems. *Water Resources Research*, 48, W03507. <https://doi.org/10.1029/2011WR011566>
- Schmid, K. S., Geiger, S., & Sorbie, K. S. (2011). Semianalytical solutions for cocurrent and countercurrent imbibition and dispersion of solutes in immiscible two-phase flow. *Water Resources Research*, 47, W02550. <https://doi.org/10.1029/2010WR009686>
- Settari, A., & Aziz, K. (1975). Treatment of nonlinear terms in the numerical solution of partial differential equations for multiphase flow in porous media. *International Journal of Multiphase Flow*, 1, 817–844.
- Silin, D., & Patzek, T. (2004). On Barenblatt's model of spontaneous countercurrent imbibition. *Transport in Porous Media*, 20(1), 161–170. <https://doi.org/10.1007/s10596-015-9555-y>
- Soriano, J., Mercier, A., Planet, R., Hernández-Machado, A., Rodríguez, M. A., & Ortín, J. (2005). Anomalous roughening of viscous fluid fronts in spontaneous imbibition. *Physical Review Letters*, 95(10), 1–4. <https://doi.org/10.1103/PhysRevLett.95.104501>
- Tang, G.-Q., & Firoozabadi, A. (2001). Effect of pressure gradient and initial water saturation on water injection in water-wet and mixed-wet fractured porous media. *SPE Reservoir Evaluation & Engineering*, 4(6), 516–524. <https://doi.org/10.2118/74711-PA>
- Tokunaga, T. K., Wan, J., Jung, J. W., Kim, T. W., Kim, Y., & Dong, W. (2013). Capillary pressure and saturation relations for supercritical CO₂ and brine in sand: High-pressure Pc(Sw) controller/meter measurements and capillary scaling predictions. *Water Resources Research*, 49, 4566–4579. <https://doi.org/10.1002/wrcr.20316>
- Vasco, DW, Pride, S. R., Zahasky, C., & Benson, S. M. (2018). Calculating trajectories associated with solute transport in a heterogeneous medium. *Water Resources Research*, 54, 6890–6908. <https://doi.org/10.1029/GRL2012-865>
- Washburn, E. W. (1921). The dynamics of capillary flow. *The Physical Review*, 17(3), 273–283. <https://doi.org/10.1103/PhysRev.17.273>
- Wickramathilaka, S., Howard, J. J., Stevens, J. C., Morrow, N. R., Mason, G., Haugen, Å., et al. (2011). Magnetic resonance imaging of oil recovery during spontaneous imbibition from cores with two-ends open boundary condition. This paper was prepared for presentation at the International Symposium of the Society of Core Analysts held in Austin, Texas, USA, 18–21 September, 2011. (SCA2011-24). <http://www.scaweb.org/assets/papers/2011&urlscore;papers/SCA2011-24.pdf>
- Zahasky, C., & Benson, S. M. (2018). Micro-positron emission tomography for measuring sub-core scale single and multiphase transport parameters in porous media. *Advances in Water Resources*, 115, 1–16. <https://doi.org/10.1016/j.advwatres.2018.03.002>
- Zhao, Y., Xue, S., Han, S., Chen, Z., Liu, S., Elsworth, D., et al. (2017). Effects of microstructure on water imbibition in sandstones using X-ray computed tomography and neutron radiography. *Journal of Geophysical Research: Solid Earth*, 122, 4963–4981. <https://doi.org/10.1002/2016JB013786>
- Zhou, X., Morrow, N., & Ma, S. (2000). Interrelationship of wettability, initial water saturation, aging time, and oil recovery by spontaneous imbibition and waterflooding. *SPE Journal*, 5(2), 21–24. <https://doi.org/10.2118/62507-PA>
- Zik, O., Moses, E., Olami, Z., & Webman, I. (1997). Scaling of propagating capillary fronts. *Europhysics Letters*, 38(7), 509–514. <https://doi.org/10.1209/epl/i1997-00104-y>
- Zimmerman, R. W., & Bodvarsson, G. S. (1989). An approximate solution for one-dimensional absorption in unsaturated porous media. *Water Resources Research*, 25(6), 1422–1428. <https://doi.org/10.1029/WR025i006p01422>
- Zimmerman, R. W., & Bodvarsson, G. S. (1991). A simple approximate solution for horizontal infiltration in a Brooks-Corey medium. *Transport in Porous Media*, 6(2), 195–205. <https://doi.org/10.1007/BF00179281>

Erratum

In the originally published version of this article, the authors mistakenly omitted some important funding information. Support from CMC-UF and award DE-SC0019165 is now acknowledged, and the present version may be considered the authoritative version of record.